$NaHCO_3$ solution, 5% w/v aqueous $NaHCO_3$ solution, and then water. Finally, the organic layer was dried over Na_2SO_4 and decanted, and the solvent was removed on a rotary evaporator. A yield of 69% (71 mg) of the dark purple microcrystals was realized. The identity and purity of the complex was verified by comparison of the IR and silica gel TLC results with those of an independently prepared sample.

$Fe_2Pt(SO)S(CO)_6(PPh_3)_2$ (6). A mixture of $Fe_2(S_2)(CO)_6$ (0.14 g, 0.41 mmol) and $Pt(PPh_3)_2(C_2H_4)$ (0.31 g, 0.41 mmol) was dissolved with CH_2Cl_2 (50 mL). The reaction mixture was stirred for 10 min, and then *m*-chloroperoxybenzoic acid (0.20 g, 1.2 mmol) was added. The red color of the reaction mixture darkened, and the solution was allowed to stir for 30 min. The solution was washed with saturated aqueous $NaHCO_3$ solution (3 × 100 mL) and then 100 mL of H_2O. The organic layer was dried over Na_2SO_4, and solids were removed via filtration. Hexanes were added to the filtrate, and the solution was concentrated to a small volume on a rotary evaporator. The product was isolated by filtration and washed with hexanes. After the product was dried in vacuo, a 62% yield (0.27 g) of red crystals was obtained. Anal. Calcd for $C_{42}H_{30}Fe_2O_7P_2PtS_2$: C, 46.72; H, 2.80; P, 5.74; S, 5.94. Found: C, 46.62; H, 2.79; P, 5.53; S, 5.86. FD-MS: *m/e* 1080 (M^+).

$[Ir(SSe)(dppe)_2]Cl$ (7). A mixture of $[Ir(dppe)_2]Cl$ (50 mg, 49 μmol) and $(MeCp)_2TiS_xSe_{5-x}$ ($x \approx 2$; 25 mg, ~50 μmol) was dissolved with 1,2-dichloroethane (20 mL). The reaction mixture was stirred for 20 min, and then the solvent was evaporated in vacuo. The solids were redissolved in CH_2Cl_2, and the iridium-containing products were isolated by gel permeation chromatography on Bio-Beads S-X4 with CH_2Cl_2 elution. The green fraction, which eluted first, was collected and the solvent removed under vacuum. ^1H NMR (360 MHz) spectroscopy indicated a mixture of products with cis stereochemistry comprised of 17% $[Ir(SSe)(dppe)_2]^+$, 75% $[Ir(Se_2)(dppe)_2]^+$, and 6% $[Ir(S_2)(dppe)_2]^+$. FD-MS for the SSe complex: *m/e* 1101 (M^+), with the signal intensities of the isotopic cluster closely matching a computer-simulated pattern. Attempts at fractional crystallization of pure $[Ir(SSe)(dppe)_2]^+$ from the product mixture were not successful.

Acknowledgment. This research was supported by the National Science Foundation (Grant CHE 81-06781). We also acknowledge financial support from the donors of the Petroleum Research Fund, administered by the American Chemical Society. NMR and mass spectral instrumentation was obtained through Grants NSF CHE79-16100 and NIH GM-27029, respectively. T.B.R. is a fellow of the A. P. Sloan and Camille and Henry Dreyfus Foundations.

Registry No. **1**, 63627-91-8; **2**, 91602-15-2; **3**, 91467-39-9; **4**, 91467-40-2; **5**, 73137-67-4; **6**, 91491-47-3; **7**, 91467-41-3; *m*-CPBA, 937-14-4; $[Ir(S_2)(dppe)_2]PF_6$, 91467-43-5; $[Ir(S_2)(dppe)_2]Cl$, 31603-13-1; $[Ir(Se_2)(dppe)_2]PF_6$, 91548-31-1; $[IrSe_2(dppe)_2]Cl$, 40603-51-8; $[Ir(dppe)_2]PF_6$, 41047-09-0; $(C_5H_5)_2Nb(S_2)Cl$, 72478-51-4; $Cp_2Nb(O)Cl$, 59412-84-9; $Fe_3(S)_2(CO)_9$, 22309-04-2; $Fe_2(S_2)(CO)_6$, 14243-23-3; $Pt(PPh_3)_2(C_2H_4)$, 12120-15-9; Se_2, 12185-17-0; S_2, 23550-45-0; CH_3CH_2SH, 75-08-1; peracetic acid, 79-21-0.

Contribution from the Department of Physics, Queen Elizabeth College, University of London, London, England, Chemical Crystallography and Inorganic Chemistry Laboratories, Oxford University, Oxford OX1 3PD, England, Department of Chemistry, University of Missouri—Rolla, Rolla, Missouri 65401, and Nuclear Physics Division, Atomic Energy Research Establishment, Harwell, Didcot OX11 0RA, England

Polarized Neutron Diffraction and Mössbauer-Effect Study of the Magnetic Ordering in Wüstite, Fe_yO

CLIVE WILKINSON, ANTHONY K. CHEETHAM,* GARY J. LONG,* PETER D. BATTLE, and DAVID A. O. HOPE

Received September 15, 1983

Samples of nonstoichiometric iron(II) oxide, Fe_yO, have been studied by polarized neutron diffraction, at 45 K, and Mössbauer spectroscopy, at 4.2 and 78 K. The neutron measurements, on samples of compositions $Fe_{0.926}O$ and $Fe_{0.943}O$, show that antiferromagnetic order is maintained in the vicinity of defect clusters. In the intercluster region the spin direction is approximately 30° from [111], but close to the defects it is about 35° from the (111) plane. The spin structure is approximately collinear at the local level. The Mössbauer spectra of a sample of composition $Fe_{0.918}O$ are extremely complex. They have been fitted to a model involving one iron(III) hyperfine sextet, two iron(II) hyperfine sextets, and an iron(III) quadrupole doublet with a very large splitting (3.8 mm s^{-1}). The doublet is ascribed to the iron(III) tetrahedral interstitials, which may be paramagnetic or spin paired with adjacent interstitials.

Introduction

Nonstoichiometric wüstite, Fe_yO, adopts the rock salt structure above its magnetic-ordering temperature. The deficienty of iron is accommodated by octahedral iron vacancies that are associated with tetrahedral interstitials to form clusters.[1] The simplest defect cluster is the 4:1 unit, containing four octahedral iron vacancies around a single tetrahedral interstitial (Figure 1a)), but X-ray and neutron diffraction measurements of the vacancy: interstitial ratio point to more extended aggregates.[2-5] Theoretical calculations favor edge-shared clusters such as the 6:2 (Figure 1b) and 8:3 units.[6] The creation of iron vacancies in iron(II) oxide is, of course, accompanied by the formation of iron(III), and in order to balance the charge locally, the iron(III) is thought to be located at the interstitial positions and in the immediate vicinity of the clusters.[6] A surprising feature of the 6:2 and related moieties is that the Fe(III)–Fe(III) distance between adjacent tetrhedral interstitials is very short (ca. 2.1 Å) and is certainly in the range where appreciable metal–metal interaction would seem likely.

The bulk magnetic properties of wüstite are well-known and indicate that it is antiferromagnetic below ca. 195 K, with the exact Néel temperature depending upon y.[7] Neutron diffraction measurements obtained below T_N show that it undergoes a rhombohedral distortion ($\alpha < 60°$) and that the bulk of the iron spins are aligned along the [111] axis of the cell; α increases with decreasing y.[1] Alternate (111) sheets are ferromagnetic and have α and β spins, respectively. A re-

* To whom correspondence should be addressed: A.K.C., Oxford University; G.J.L., University of Missouri—Rolla.

(1) Roth, W. L. *Acta Crystallogr.* **1960**, *13*, 40.
(2) Koch, F.; Cohen, J. B. *Acta Crystallogr., Sect. B* **1969**, *B25*, 275.
(3) Cheetham, A. K.; Fender, B. E. F.; Taylor, R. I. *J. Phys. C* **1971**, *4*, 2160.
(4) Gavarri, J. R.; Carel, C.; Weigel, D. *J. Solid State Chem.* **1979**, *29*, 81.
(5) Gavarri, J. R.; Weigel, D.; Carel, C. *J. Solid State Chem.* **1981**, *36*, 255.
(6) Catlow, C. R. A.; Fender, B. E. F. *J. Phys. C.* **1975**, *8*, 3267.
(7) Koch, F.; Fine, M. E. *J. Appl. Phys.* **1966**, *38*, 1470.

0020-1669/84/1323-3136$01.50/0

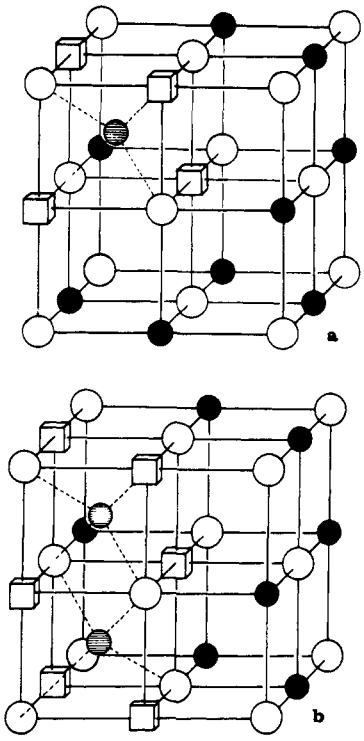

Figure 1. Defect clusters in Fe_yO: (a) an isolated 4:1 cluster; (b) a 6:2 cluster with a common shared edge. Filled circles are octahedral iron atoms, shaded circles are tetrahedral iron interstitials, open circles are oxygen atoms, and cubes are octahedral vacancies.

markable feature of the neutron results is that the magneic neutron scattering from the octahedral iron atoms falls well below that expected on the basis of the measured occupancy numbers, and Battle and Cheetham[8] have proposed that the spins in the cluster and its immediate environs lie in the (111) plane and are ferromagnetically arranged, with the tetrahedral interstitials coupled antiferromagnetically to the nearest-neighbor, octahedral iron sites; the spins within the cluster do not appear to contribute to the coherent magnetic scattering.

We have now undertaken a detailed study of the magnetic properties of Fe_yO by Mössbauer spectroscopy and the scattering of polarized neutrons. The results are at variance with existing models and shed new light on the low-temperature behavior of wüstite.

Experimental Section

The samples were prepared and characterized by the methods reported previously.[8] X-ray power diffraction studies indicated the absence of Fe_3O_4, and only lines attributable to Fe_yO were observed.

The Mössbauer-effect absorbers, prepared by mixing fine powders with Vaseline to remove any potential crystallite orientation effects, contained ca. 50 mg of sample/cm^2. The spectra were obtained on either a Ranger Electronics or a Harwell constant-acceleration spectrometer, each of which used a room-temperature rhodium-matrix source and was calibrated at room temperature with natural α-iron foil. Liquid-helium-temperature spectra were obtained in a cryostat in which the samples were placed directly into liquid helium. Least-squares minimization programs implemented on the Amdahl 7 at the University of Missouri–Rolla were used to analyze the spectra.

Neutron polarization analysis measurements were made with neutrons of wavelength 0.84 Å on the D5 diffractometer at the Institut Laue-Langevin, Grenoble, France. The technique employed was that described by Ziebeck and Brown,[9] which allows magnetic contributions to the diffuse scattering to be separated from nuclear contributions by measuring the difference between the spin-flip cross sections when the incident neutron polarization vector is parallel to $\sigma_\parallel{}^{+-}$ and perpendicular to $\sigma_\perp{}^{+-}$, the scattering vector. The sample was maintained at 45 K in a Displex refrigerator, and a neutron powder diffraction pattern showing the expected magnetic and nuclear Bragg peaks was recorded out to $2\theta = 30°$. Spin flip cross section measurements were then made at 2θ intervals of 1° from 2° to 27°, avoiding regions in which Bragg reflections had previously been observed. Sets of measurements were taken with an applied magnetic field, and hence the neutron polarization direction, parallel to and then perpendicular to the scattering vector, which was always in the horizontal plane. The difference magnetic cross section ($\sigma_\parallel{}^{+-} - \sigma_\perp{}^{+-}$) for $Fe_{0.926}O$, which is shown in Figure 2, has been placed on an absolute scale by using the observed and calculated intensity of the strong nuclear (200) Bragg peak. Similar results were obtained for a sample of composition $Fe_{0.943}O$.

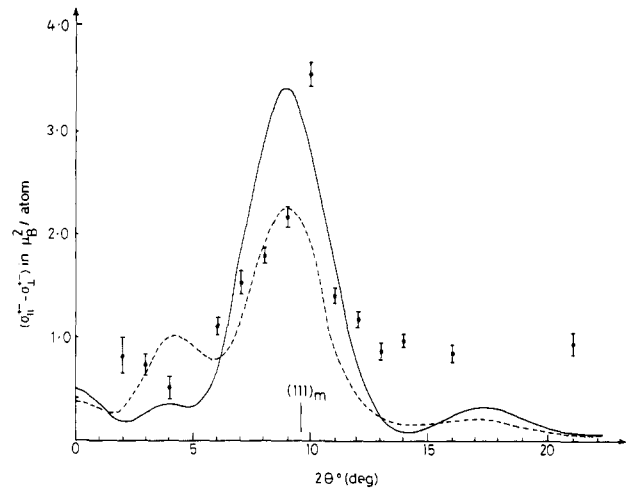

Figure 2. Neutron-scattering data observed at 45 K from $Fe_{0.926}O$ by polarization analysis. Intensities have been scaled to $\mu_B{}^2$ per iron atom in the sample, and the position of the (111) Bragg reflection from the extended FeO magnetic structure is indicated. Curves calculated for the magnetic scattering cross section per iron atom in a 12-Å diameter FeO cluster are also shown. The full curve is for a cluster with no defects and the dashed curve for a cluster with an 8:3 defect at its center.

Results and Discussion

Neutron Diffraction Data. The derivation of the expression for the calculation of the intensity of scattering from noninteracting finite clusters of atoms having a common spin direction is given in Appendix I.

The appropriate parameters to be used in calculating the scattering from the direct clusters in Fe_yO can be obtained from the composition of the oxide and the observed neutron diffraction pattern. In $Fe_{0.926}O$, the concentration of defects is sufficiently high that all atoms can be considered to be part of a defect cluster in which the average number of iron atoms, if all defects are of the 4:1 type, is 40, rising to 68 if the defects are of the 8:3 type. The average cluster "diameter" and intercluster distance is therefore in the region of 12 Å.

Information on the direction of spins is contained in the polarized neutron-scattering data in Figure 2. The absence of any appreciable scattering in the forward direction indicates that the clusters are approximately antiferromagnetic. The broad peak in the region of the forbidden {111} magnetic Bragg reflection indicates that rhombohedral configurational symmetry is retained in the cluster but that the moments of the iron atoms deviate from a [111] direction.

In our calculation we have therefore used a model in which alternate (111) sheets of iron atoms with equal moments of 4.2 μ_B are antiferromagnetically coupled. Near the center of the cluster, the moment direction is close to the (111) plane but rotates toward the [111] direction between the clusters (Figure 3). For simplicity of calculation, the planar component has been described by a Gaussian function centered on the defect and having a full width at half-height of 12 Å. The scattered intensity per atom, calculated for a 12-Å di-

(8) Battle, P. D.; Cheetham, A. K. *J. Phys. C.* **1979**, *12*, 337.
(9) Ziebeck, K. R. A.; Brown, P. J. *J. Phys. F.* **1980**, *10*, 2015.

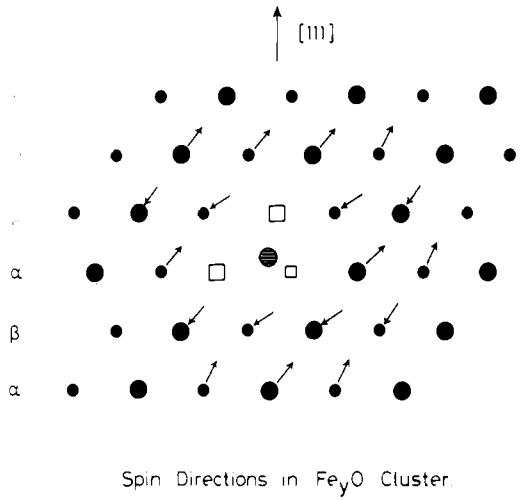

Figure 3. Projection of two adjacent (110) layers of metal atoms, shown as large and small circles, respectively, displaying the spin arrangement around a defect cluster in Fe_yO. Alternate (111) layers of metal atoms are labeled α and β.

ameter cluster, is shown in Figure 2. Curves are given for a cluster with no defects and for one with an 8:3 cluster at its center. No moments have been associated with vacant lattice sites or with interstitial atoms. Intensities calculated for 4:1 and 6:2 clusters lie between these curves. No instrumental broadening has been folded into the calculated function; the broadening corresponds only to about one-tenth of the width of the main peak. We do not expect to see any structure in the pattern due to inelastically scattered neutrons (as studied in wüstite single crystals by Kugel et al.[10]), because the scattering cross section for a powder sample is so small and the 10.5-THz energy acceptance of the D5 spectrometer is so wide; we estimate these processes will give only a low contribution to the background.

The most striking feature of the model shown in Figure 3 is that the spins are approximately collinear, at variance with previous models[8] but in accordance with the results on the rock salt solid solutions $Mn_{1-x}Ni_xO$[11] and $Co_{1-x}Ni_xO$.[12] In the intercluster region the spin direction is approximately 30° from [111], but close to the defects it is 35° from the (111) plane. On a first consideration, the magnetic structure is rather like that of CoO, in which the collinear spin direction lies between [001] and the (111) plane,[13] but the absence of a sharp {111} magnetic reflection indicates that the transverse (in the (111) plane) component of the spin, unlike the axial component, does not achieve long-range rrder. However, the transverse spin component does undergo short-range ordering on a scale that is significantly larger than the size of the magnetic cluster. This leads to coherence in the scattering from adjacent magnetic clusters, and we presume that it is this that is responsible for the sharper peak that appears at ca. 10° in 2θ and the intensity that is evident beyond 13° in 2θ in the observed pattern; these effects have not been treated in the present calculation. Magnetic ordering similar to that embodied in our model has recently been observed in the system $K_2Co_xFe_{1-x}F_4$.[14] The cluster model is also consistent with the magnetic occupation number of 0.64 previously measured by Battle and Cheetham.[8] The average axial component of the iron atoms in the cluster is 2.6 μ_B, which translates into an

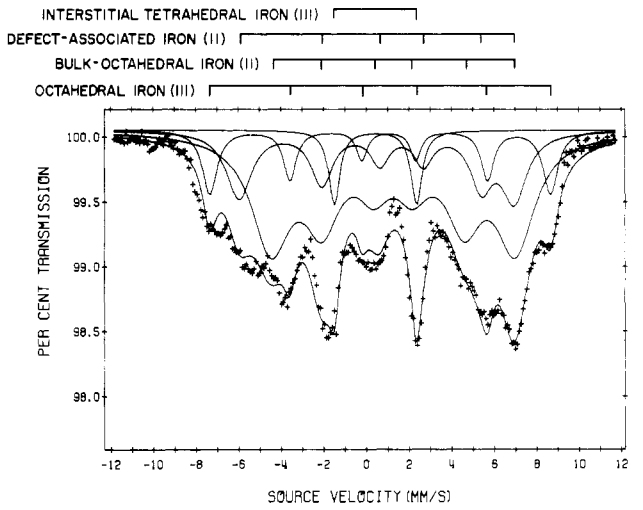

Figure 4. Mössbauer spectrum of $Fe_{0.918}O$ obtained at 78 K. The fit corresponds to model 1.

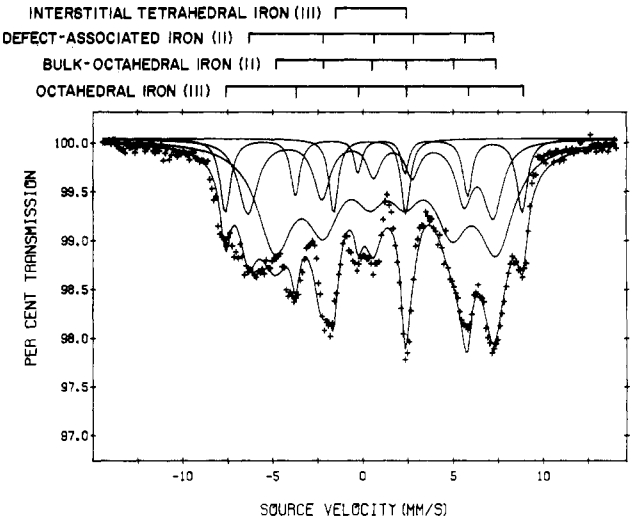

Figure 5. Mössbauer spectrum of $Fe_{0.918}O$ obtained at 4.2 K. The fit corresponds to model 1.

apparent magnetic occupation number of 0.62. We therefore believe that our model is consistent with the principal features of the neutron results, and we must now use the Mössbauer data to obtain information about the magnetic behavior of the tetrahedral interstitial atoms.

Mössbauer-Effect Spectral Data. The Mössbauer spectrum of $Fe_{0.918}O$ obtained at room temperature has been reported earlier[15] and was interpreted in terms of a singlet due to iron(III) and two quadrupole-split doublets, which were attributed to iron(II) in octahedral sites either in the bulk or near the interstitial clusters. The Mössbauer-effect spectra obtained at 78 and 4.2 K are shown in Figures 4 and 5 and are qualitatively similar to those reported earlier.[16] These spectra are extremely complex and consist of many overlapping unresolved magnetic sextets. Very similar spectra were obtained[17] for the related $(Mn_xFe_{1-x})_yO$ samples, and their simultaneous study proved very helpful in modeling the spectrum of $Fe_{0.918}O$. Repeated attempts to fit these spectra with up to six magnetic sextets proved impossible with any realistic model. In no case was it possible to fit the observed strong

(10) Kugel, G. E.; Hennion, B.; Carabatos, C. *Phys. Rev. B.* **1978**, *18*, 1317.
(11) Cheetham, A. K.; Hope, D. A. O. *Phys. Rev. B* **1983**, *27*, 6964.
(12) Battle, P. D.; Cheetham, A. K.; Gehring, G. A. *J. Appl. Phys.* **1979**, *50*, 7578.
(13) Herrmann-Ronzaud, D.; Burlet, P.; Rossat-Mignod, J. *J. Phys. C* **1978**, *11*, 2123.
(14) Vlak, W. A. H. M.; Frikkee, E.; Arts, A. F. M.; de Wijn, H. W. *J. Phys. C*, in press.
(15) Hope, D. A. O.; Cheetham, A. K.; Long, G. J. *Inorg. Chem.* **1982**, *21*, 2804.
(16) Greenwood, N. N.; Howe, A. T. *J. Chem. Soc., Dalton Trans.* **1972**, 110.
(17) Long, G. J.; Cheetham, A. K.; Hope, D. A. O. *Inorg. Chem.*, following paper in this issue.

lines at ca. −1.5 and 2.5 mm/s on the basis of magnetic sextets. The same problem was encountered with each of the $(Mn_xFe_{1-x})_yO$ spectra.[17] It was noted, however, that samples that were high in manganese content and very low in defect content did not exhibit these lines.[18] It was therefore decided to fit these two lines to either two singlets or to a quadrupole doublet. In this case, a reasonable fit was obtained immediately and it was found that the area of the resulting doublet had the approximate relative area that would be expected of the interstitial tetrahedral iron(III) as determined from neutron-scattering studies.[15]

The final model that was used to fit these spectra consisted of three magnetic sextets and a quadrupole doublet. Because the model contains so many adjustable parameters, it is necessary to build as many constraints into the fitting procedure as possible. In all models, each magnetic sextet was fitted on the basis of an adjustable isomer shift, δ, internal hyperfine field, H_{int}, quadrupole shift, QS, and line width, Γ_1, which was the width of the outer magnetic lines. The line widths of lines 2 and 5 were ca. $\Gamma_1 - 0.5\Delta\Gamma$ and the line widths of lines 3 and 4 were ca. $\Gamma_1 - \Delta\Gamma$ where $\Delta\Gamma$ was determined from preliminary fits and was not refined. The relative areas of the lines in each component were constrained in the ratio of 3:2:1:1:2:3, as required for an unoriented powder sample. The relative areas of each separate spectral component were calculated for a 6:2 cluster from the stoichiometry of the compound and the vacancy concentration, and in model 1 these relative areas were constrained. In model 2, the relative areas of the sextets were fixed but the area of the doublet was unconstrained. In model 3, the area of each component was unconstrained. The hyperfine parameters obtained for each model and each component are given in Table I, and the fits obtained for model 1 are shown in Figures 4 and 5. The fits and parameters obtained for models 1 and 2 were virtually identical whereas model 3 tended to decrease the relative area of one sextet (attributed to the bulk iron(II); see below) but gave very similar areas for the doublet and very similar hyperfine parameters—see Table I. Two things are immediately obvious from an evaluation of these fits and Figures 4 and 5. First, although the fits are reasonable, they are far from exact. Second, the line widths of the magnetic components are very high. Both of these observations no doubt result from the excess simplicity of our model, and indeed better fits can be obtained with additional magnetic components but always with the requirement of the doublet. Because the results seem chemically reasonable on the basis of a simple model for a very complex magnetic material, we have elected to proceed with this model. The results for the analogous manganowüstites will be discussed in detail elsewhere.[17]

The hyperfine parameters for each of the components seem reasonable in terms of our knowledge of the chemical, magnetic, and electronic structure of Fe_yO. The magnetic component with the highest internal hyperfine field is assigned to the substitutional octahedral high-spin iron(III), which is associated with the defect cluster to provide charge neutrality. Its internal hyperfine field (510 kOe at 4.2 K) is reasonable for the saturation field of iron(III) in a material such as wüstite with a significant covalent contribution to the bonding, which will lower the saturation field from the expected ca. 550 kOe.[19] The isomer shift of ca. 0.8 mm/s seems somewhat high, but the adjacent cation vacancies may be very effective in permitting the expansion of the *n*s functions on the iron(III), thus increasing the iron(III) isomer shift. The relatively small quadrupole shift of ca. +0.2 mm/s probably results from a lattice contribution to the electric field gradient at the iron(III)

Table I. Mössbauer-Effect Spectral Data for $Fe_{0.918}O$[a]

		296 K					78 K					4.2 K					
site	model[b]	δ	ΔE_Q	Γ	%*A*	χ^2	δ	Q[c]	H_{int}	Γ_1	$\Delta\Gamma$	%*A*	χ^2	δ	Q[c]	H_{int}	Γ_1	$\Delta\Gamma$	%*A*	χ^2
octahedral iron(III)	1	0.54		0.58	12.5	4.28	0.86	+0.20	495	0.83	0.14	12.5	3.40	0.81	+0.21	510	0.70	0.20	12.5	4.55
	2	0.44		0.58	12.9	3.92	0.86	+0.20	496	0.83	0.14	12.5	3.43	0.81	+0.21	510	0.70	0.20	12.5	4.55
	3	0.42		0.37	10.0	3.23	0.84	+0.18	494	1.13	0.32	19.6	2.86	0.79	+0.21	512	0.71	0.20	12.5	4.45
defect associated octahedral iron(II)	1	0.86	0.74	0.32	23.1		1.07	+0.59	400	1.44	0.41	23.1		1.03	+0.63	421	1.29	0.37	23.1	
	2	0.87	0.71	0.33	23.9		1.07	+0.59	400	1.44	0.41	23.1		1.03	+0.63	421	1.29	0.37	23.1	
	3	0.89	0.68	0.33	24.0		1.15	+0.49	395	1.65	0.47	34.6		1.03	+0.63	422	1.25	0.36	23.1	
bulk octahedral iron(II)	1	1.05	0.62	0.49	59.0		1.26	−0.01	355	2.23	0.37	59.0		1.30	+0.05	380	2.39	0.40	59.0	
	2	1.05	0.61	0.49	61.3		1.25	−0.01	355	2.23	0.37	58.9		1.29	+0.05	380	2.40	0.41	59.0	
	3	1.05	0.61	0.48	60.8		1.19	−0.07	345	1.78	0.30	39.1		1.27	+0.05	381	2.49	0.42	58.9	
interstitial tetrahedral iron(III)	1	0.63	0.94	0.35	5.4		0.43	3.84	0	0.62		5.4		0.37	3.98	0	0.59		5.4	
	2	0.60	1.00	0.20	1.8		0.43	3.84	0	0.62		5.5		0.37	3.98	0	0.59		5.4	
	3	0.60	0.99	0.31	4.3		0.46	3.83	0	0.62		6.6		0.37	4.01	0	0.56		5.5	

[a] All data except H_{int} in mm/s relative to room-temperature natural α-iron foil. H_{int} is in kOe. [b] The models are defined in the text. [c] Q is the quadrupole shift for the magnetic components and the magnitude of the quadrupole interaction for the nonmagnetic component.

(18) Long, G. J., unpublished data.
(19) Johnson, C. E. In "Hyperfine Interactions in Excited Nuclei"; Goldring, G., Kalish, R., Eds.; Gordon and Breach: New York, 1971.

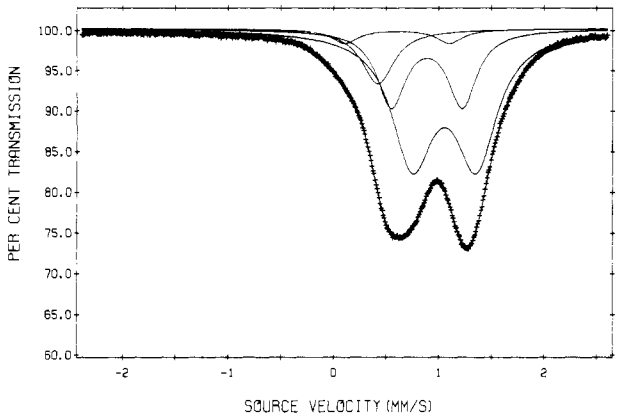

Figure 6. Mössbauer spectrum of $Fe_{0.918}O$ obtained at 297 K. The fit corresponds to model 1.

site adjacent to the defect cluster. The two remaining magnetic sextets, with higher isomer shifts, are assigned to octahedral high-spin iron(II). The sextet with the higher field is attributed to iron(II) that is adjacent to the cluster and hence associated with the substitutional iron(III), which would produce a larger hyperfine field at the iron(II). Again, the isomer shift for this site is somewhat lower than that expected for iron(II) in an oxide lattice because of the near-neighbor cation vacancies, which also produce the large observed quadrupole shift found in this component. The observed saturation hyperfine field of 421 kOe found at 4.2 K is reasonable for iron(II) associated with a vacancy and substitutional iron(III). The second iron(II) magnetic sextet has a typical isomer shift and a smaller quadrupole shift, as would be expected for an iron(II) ion located in the "bulk" of the rock salt FeO structure. The large line width of this site no doubt results from a distribution of hyperfine fields in the "bulk" arising from the numerous defects distributed throughout this material.

By far the most interesting component in our fit is the doublet that we attribute to the interstitial tetrahedral iron(III) ions. The area of this component remains essentially the same in all three of our models and is close to that expected for the interstitial component as given in Table I for model 1. In all cases, the isomer shift of ca. 0.40 mm/s is very reasonable for tetrahedral high-spin iron(III) in an oxide lattice.[20] The most unusual hyperfine parameter is the quadrupole interaction of ca. 3.8 mm/s, a value much higher than is normally found in tetrahedral high-spin iron(III) compounds. This large quadrupole interaction must result from a substantial lattice component in the electric field gradient at the iron(III) site; any valence component would be small for the high-spin d^5, ^6A, electronic configuration expected in this case. It is now possible to reinterpret the room-temperature spectrum[15] of $Fe_{0.918}O$ in terms of this model, and as illustrated in Figure 6 and Table I, we observe a doublet with a smaller, but nevertheless rather high, value of ΔE_Q (ca. 1.0 mm/s), which is assigned to the tetrahedral iron(III) site. This must reflect a lattice contribution to the EFG tensor arising from the presence of the adjacent tetrahedral iron(III) interstitial in the same cluster. We believe that the appearance of a doublet with enhanced splitting at low temperature must result from two factors. Above the magnetic-ordering temperature (195 K) the material is cubic with space group $Fm3m$, but below T_N, the material undergoes a phase change to a rhombohedral structure ($R\bar{3}$) in which the local site symmetry at the iron(III) interstitial will be lower. Second, there is evidence at room temperature for iron(II)–iron(III) electron transfer in the neighboring octahedral sites[15] that will vanish at low temperatures, giving an additional contribution to the EFG tensor. Although a value of 3.8 mm/s is large, similar large lattice contributions to the EFG tensor have been observed in other iron(III) oxides[21] and iron(III) complexes.[22]

The Mössbauer results indicate that the tetrahedral interstitial iron(III) ions are not coupled to the antiferromagnetic ordering of the bulk structure. One possible explanation for this is that the ions are paramagnetic because they experience contradictory exchange fields from the surrounding octahedral ions. This must be the case for any isolated 4:1 clusters (Figure 1a). For a 6:2 cluster (Figures 1b), antiferromagnetic coupling[23] of the unpaired spins on the two iron(III) interstitials may result from a combination of both direct metal–metal interaction and superexchange through the bridging oxide ions. This type of molecular magnetic coupling will lead to no net unpaired spin at the interstitial iron(III) ion and hence no internal hyperfine field as is observed in the Mössbauer spectra (see Table I and Figures 4 and 5). Because of the short iron(III)–iron(III) distance of ca. 2.15 Å, the exchange coupling constant must be negative and rather large in magnitude. This would indicate that, at least at 4.2 K, the interstitial iron(III) ions are essentially diamagnetic in nature. Our present neutron results, and those obtained previously by using unpolarized neutrons, lack the sensitivity to determine the magnetic characteristics of the tetrahedral interstitial, which represents only ca. 4% of the total iron.

It is interesting to summarize the complementarity of the two techniques used in this study. The polarized neutron results yield information about the spin arrangement around the defect cluster, but they shed little light on the magnetic nature of the interstitials. The Mössbauer results are sensitive to the latter and also provide further evidence that the atomic arrangement within the defect clusters has been correctly deduced in previous room-temperature studies using neutron diffraction and Mössbauer spectroscopy.[15]

Acknowledgment. It is a pleasure to acknowledge the assistance of and helpful discussions with Drs. T. E. Cranshaw, A. Gérard, F. Grandjean, G. Longworth, and K. Zieback and B. Laundy. We thank the Science and Engineering Research Council for the provision of the neutron facilities at ILL, Grenoble, and a research studentship for D.A.O.H., NATO, for a cooperative scientific research grant, and the USAF for a support grant (AFOSR-79-0120). P.D.B. thanks St. Catherine's College, Oxford, and the CEGB for the award of a research fellowship.

Appendix I

For a cluster of N magnetic ions in positions $\mathbf{r}_i$ with spins S_j and a common spin direction $\hat{\eta}$ the magnetic structure factor may be defined as $\mathbf{M}(\mathbf{k}) = \sum_i^N S_i \hat{\eta} f_i(\mathbf{k}) e^{2\pi i \mathbf{r}_i \mathbf{k}}$, where $f_i(\mathbf{k})$ is the form factor for the scattering vector $\mathbf{k}$. The neutron spin-flip scattering cross section σ^{+-} for such a cluster contains both nuclear and magnetic contributions. The magnetic contribution is related to $\mathbf{M}(\mathbf{k})$ through the magnetic interaction vector $\mathbf{Q}_\perp(\mathbf{k}) = \mathbf{k} \wedge (\mathbf{M}(\mathbf{k}) \wedge \hat{\mathbf{k}})$ and is proportional to $|\mathbf{Q}_\perp(\mathbf{k}) \wedge \hat{\lambda}|^2$, where $\hat{\lambda}$ is the neutron polarization direction.

In the present experiment, when the magnetic field is applied parallel to $\mathbf{k}$ (horizontally), $\hat{\lambda}$ is parallel to $\mathbf{k}$ and the spin-slip scattering cross section $\sigma_\parallel^{+-}$ is therefore proportional to $|\mathbf{Q}_\perp(\mathbf{k})|^2$. When the field is applied vertically, both $\mathbf{Q}_\perp(\mathbf{k})$ and $\hat{\lambda}$ lie in the plane perpendicular to $\mathbf{k}$ and the magnitude of the cross section $\sigma_\perp^{+-}$ is dependent on $|\mathbf{Q}_\perp(\mathbf{k}) \wedge \hat{\lambda}|^2$. Crystallites (and therefore clusters) with all orientations are present in the

(20) Greenwood, N. N.; Gibb, T. C. "Mössbauer Spectroscopy"; Chapman and Hall: London, 1971.
(21) Rao, P. M.; Gérard, A.; Grandjean, F. *Phys. Status Solidi A* **1979**, *54*, 529.
(22) Fitzsimmons, B. W.; Johnson, C. E. *Chem. Phys. Lett.* **1974**, *24*, 422.
(23) Boudreaux, E. A.; Mulay, L. N. "Theory and Applications of Molecular Paramagnetism"; Wiley: New York, 1976.

powdered sample, and for a particular $\mathbf{Q}_\perp(\mathbf{k})$ the average value of $|\mathbf{Q}_\perp(\mathbf{k}) \wedge \hat{\lambda}|^2$ taken over the plane is $^1/_2|\mathbf{Q}_\perp(\mathbf{k})|^2$. The nuclear contributions to $\sigma_\parallel^{+-}$ and $\sigma_\perp^{+-}$ are identical, and the difference $(\sigma_\parallel^{+-} - \sigma_\perp^{+-})$ is therefore proportional to $^1/_2|\mathbf{Q}_\perp(\mathbf{k})|^2$.

The expression $|\mathbf{Q}_\perp(\mathbf{k})|^2$ may be expanded as

$$|\mathbf{Q}_\perp(\mathbf{k})|^2 = \sum_i^N \sum_j^N f^2(\mathbf{k})\, S_i S_j \sin^2 \tau\, e^{2\pi i \mathbf{r}_{ij}\cdot\mathbf{k}}$$

where $\mathbf{r}_{ij}$ is the interatomic vector between the i^{th} and j^{th} magnetic ions, τ is the angle between $\mathbf{k}$ and $\hat{\eta}$, and $f(\mathbf{k})$ is assumed to be the same for every ion. Because all possible orientations of cluster and hence of $\hat{\eta}$ are present, $|\mathbf{Q}_\perp(\mathbf{k})|^2$ must be spherically averaged. Assuming that $f(\mathbf{k})$ is spherically symmetric, the averaged value can be shown to be

$$|\mathbf{Q}_\perp(\mathbf{k})|^2 = \sum_i^N \sum_j^N S_i S_j f^2(\mathbf{k}) \left[\left(\frac{\sin(2\pi r_{ij}k)}{2\pi r_{ij}k} \right) \sin^2 \beta_{ij} - \Phi(2\pi r_{ij}k)(3\cos^2 \beta_{ij} - 1) \right]$$

where β_{ij} is the angle between $\hat{\eta}$ and $\mathbf{r}_{ij}$ and $\Phi(x) = (x\cos x - \sin x)/(x^3)$. (The equivalent Debye formula for the nuclear scattered intensity would be $|F(\mathbf{k})|^2 = \sum_i^N \sum_j^N b_i b_j [(\sin(2\pi r_{ij}k))/2\pi r_{ij}k]$.)

In the case of FeO clusters there are three trigonally equivalent directions in the (111) plane in which $\hat{\eta}$ can lie. Assuming these are equally probable, $|\mathbf{Q}_\perp(\mathbf{k})|^2$ can be averaged over these three domains to give

$$|\mathbf{Q}_\perp(\mathbf{k})|^2 = \sum_i \sum_j S_i S_j f^2(\mathbf{k}) \left[\left(\frac{\sin(2\pi k r_{ij})}{2\pi k r_{ij}} \right) \times \left(1 - \frac{1}{2}\sin^2 \delta_{ij} \right) - \Phi(2\pi k r_{ij}) \left(\frac{3}{2}\sin^2 \delta_{ij} - 1 \right) \right]$$

where δ_{ij} is the angle between $\mathbf{r}_{ij}$ and the [111] direction. Components of the spin parallel to [111] also give a contribution to the scattering, which is

$$|\mathbf{Q}_\perp(\mathbf{k})|^2 = \sum_i \sum_j [(S^2 - S_i^2)(S^2 - S_j^2)]^{1/2} f^2(\mathbf{k}) \times \left[\left(\frac{\sin(2\pi r_{ij}k)}{2\pi r_{ij}k} \right) \sin^2 \delta_{ij} - \Phi(2\pi k r_{ij})(3\cos^2 \delta_{ij} - 1) \right]$$

where S is the full spin associated with the iron atoms. A more reasonable assumption in this case is that the axial components are coherent with those parallel to [111] in the nearby clusters, in which case, by employing Babinet's principle it can be shown that the term $[(S^2 - S_i^2)(S^2 - S_j^2)]^{1/2}$ in the above expression should be replaced by $[S - (S^2 - S_i^2)^{1/2}][S - (S^2 - S_j^2)^{1/2}]$.

Registry No. Wüstite, 17125-56-3.

Contribution from the Department of Chemistry, University of Missouri—Rolla, Rolla, Missouri 65401, Chemical Crystallography Laboratory, Oxford University, Oxford OX1 3PD, England, and Nuclear Physics Division, Atomic Energy Research Establishment, Harwell, Didcot OX11 0RA, England

Neutron Diffraction and Mössbauer-Effect Study of $(Mn_xFe_{1-x})_yO$ Solid Solutions

GARY J. LONG,* D. A. O. HOPE, and A. K. CHEETHAM*

Received September 15, 1983

The nonstoichiometric solid solutions $(Mn_xFe_{1-x})_yO$ have been studied at low temperatures by Mössbauer spectroscopy and Rietveld analysis of powder neutron diffraction data. For $x < 0.23$, the neutron measurements show that the spin direction is between the [111] axis and the (111) plane, as in Fe_yO itself, but for $x > 0.23$ the spins appear to lie in the (111) plane. Except for samples with y close to unity, the coherent magnetic scattering is less than expected, indicating that long-range magnetic ordering is not complete. The Mössbauer spectra of samples containing large concentrations of iron(III) are very complex and are fitted to a model with three hyperfine sextets, two for octahedral iron(II) and one for octahedral iron(III), and a quadrupole doublet for tetrahedral iron(III). For samples containing almost no iron(III), the spectra were fitted to a model with three iron(II) sextets, corresponding to sites with differing numbers of manganese neighbors.

Introduction

The monoxides of manganese and iron adopt the rock salt structure and are completely miscible at temperatures above 900 °C, as illustrated in the phase diagram[1] presented in Figure 1. Iron(II) oxide is nonstoichiometric, accommodating a deficiency of iron by the formation of iron vacancies and a small number of iron interstitials.[2] These defects aggregate to form the tetrahedral units[3] shown in Figure 2a, which are believed to condense by edge sharing to form larger units such as the 6:2 vacancy to interstitial cluster[4] shown in Figure 2b. Below 570 °C, iron(II) oxide disproportionates into iron metal and Fe_3O_4.[5] The solid solutions, $(Mn_xFe_{1-x})_yO$, can be quenched to room temperature, and our recent examination of these materials by neutron diffraction and Mössbauer spectroscopy has shown that their defect structure is similar to that of Fe_yO, itself.[6]

On cooling below room temperature, Fe_yO and MnO become antiferromagnetically ordered with Néel temperatures of ca. 200 and 118 K, respectively.[7,8] In both cases, the onset of magnetic ordering is accompanied by a rhombohedral distortion, which may be expressed in terms of the rhombohedral distortion angle, α; Fe_yO has α less than 90° and the spin apparently directed along the [111] axis,[9] whereas MnO has α greater than 90° with the spin lying in the (111) plane.[10]

* To whom correspondence should be addressed: G.J.L., University of Missouri—Rolla; A.K.C., Oxford University.

(1) Tret'yakov, Y. D.; Saksonov, Y. G.; Gordeev, I. V. *Inorg. Mater.* (*Engl. Transl.*) **1965**, *1*, 382.
(2) Roth, W. L. *Acta Crystallogr.* **1960**, *13*, 40.
(3) Cheetham, A. K.; Fender, B. E. F.; Taylor, R. I. *J. Phys. C* **1971**, *4*, 2160.
(4) Catlow, C. R. A.; Fender, B. E. F. *J. Phys. C* **1975**, *8*, 3267.
(5) Fender, B. E. F.; Riley, F. D. *J. Phys. Chem. Solids* **1969**, *30*, 793.
(6) Hope, D. A. O.; Cheetham, A. K.; Long, G. J. *Inorg. Chem.* **1982**, *21*, 2804.
(7) Koch, F.; Fine, M. E. *J. Appl. Phys.* **1966**, *38*, 1470.
(8) Boire, R.; Collins, M. F. *Can. J. Phys.* **1977**, *55*, 688.
(9) Shull, C. G.; Strauser, W. A.; Wollan, E. O. *Phys. Rev.* **1951**, *83*, 333.
(10) Bidaux, R.; Conte, R.; Nasser, J. A. *J. Phys.* (*Orsay, Fr.*) **1980**, *41*, 1317.

0020-1669/84/1323-3141$01.50/0